SHORT COMMUNICATION

Improved identification of DNA double strand breaks: γ-H2AX-epitope visualization by confocal microscopy and 3D reconstructed images

Nico Ruprecht[1,2] · Martin N. Hungerbühler[1,2] · Ingrid B. Böhm[1,2] · Johannes T. Heverhagen[1,2]

Abstract

Currently, in the context of radiology, irradiation-induced and other genotoxic effects are determined by visualizing DSB-induced DNA repair through γ-H2AX immunofluorescence and direct counting of the foci by epifluorescence microscopy. This procedure, however, neglects the 3D nature of the nucleus. The aim of our study was to use confocal microscopy and 3D reconstructed images to improve documentation and analysis of γ-H2AX fluorescence signals after diagnostic examinations. Confluent, non-dividing MRC-5 lung fibroblasts were irradiated in vitro with a Cs-137 source and exposed to radiation doses up to 1000 mGy before fixation and staining with an antibody recognizing the phosphorylated histone variant γ-H2AX. The 3D distribution of γ-H2AX foci was visualized using confocal laser scanning microscopy. 3D reconstruction of the optical slices and γ-H2AX foci counting were performed using Imaris Image Analysis software. In parallel, γ-H2AX foci were counted visually by epifluorescence microscopy. In addition, whole blood was exposed ex vivo to the radiation doses from 200 to 1600 mGy. White blood cells (WBCs) were isolated and stained for γ-H2AX. In fibroblasts, epifluorescence microscopy alone visualized the entirety of fluorescence signals as integral, without correct demarcation of single foci, and at 1000 mGy yielded on average 11.1 foci by manual counting of 2D images in comparison to 36.1 foci with confocal microscopy and 3D reconstruction ($p < 0.001$). The procedure can also be applied for studies on WBCs. In contrast to epifluorescence microscopy, confocal microscopy and 3D reconstruction enables an improved identification of DSB-induced γ-H2AX foci, allowing for an unbiased, ameliorated quantification.

Keywords γ-H2AX foci · DNA DSBs · Confocal microscopy · 3D reconstructed images

Introduction

Maintaining the genome integrity and stability is one central function of all cells. In particular, in higher organisms, mutations on the basis of DNA double strand breaks (DSBs) may be harmful, because they could be the origin of cancer (Berrington de Gonzalez and Darby 2004; Lobrich and Jeggo 2007). Knowledge about genotoxicity, its sources, the principle of DNA-repair mechanisms, and the analysis

of DNA DSBs is very important to either increase (treatment regimens in oncology) or to minimize its influence. The latter is aimed at diagnostic radiologic X-ray-based procedures: an as-much-as-possible minimalized degree of radiation-induced DNA damage is mandatory in CT-scans and interventional procedures.

DNA damage includes a wide range of DNA base modifications, single-strand breaks (SSBs) and DSBs, which are a threat to genome stability (Tounekti et al. 2001). To maintain genome stability, there are several cellular repair mechanisms operating (Symington and Gautier 2011). If DSBs occur due to exogenous agents, such as ionizing radiation or during programmed recombination events, one of the first observed cellular responses is the rapid phosphorylation of the histone protein H2AX at serine 139 (Burma et al. 2001; Rogakou et al. 1998; Chen et al. 2000). Phosphorylation of H2AX involves the phosphatidylinositol 3-kinase family consisting of ataxia telangiectasia mutated (ATM), DNA-dependent protein kinase, ataxia telangiectasia and

Ingrid B. Böhm, Johannes T. Heverhagen are contributed equally.

✉ Nico Ruprecht
nicoolivier.ruprecht@insel.ch

1 Department of Diagnostic, Interventional, and Pediatric Radiology, Inselspital, Bern University Hospital, University of Bern, Freiburgstrasse 10, 3010 Bern, Switzerland

2 Department of BioMedical Research, University of Bern, Bern, Switzerland

Rad3-related (ATR) kinases (Ward and Chen 2001; Stiff et al. 2004; Wang et al. 2005). The phosphorylated H2AX, termed γ-H2AX, is recognized by a specific antibody and serves as a molecular marker to visualize the onset of DNA DSB-induced DNA repair (Pilch et al. 2003; Sedelnikova et al. 2002). Various techniques are known to visualize γ-H2AX. The intensity of the fluorescence labelled anti-γ-H2AX antibody is measured by fluorescence-activated cell sorting or by counting foci using epifluorescence microscopy (Muslimovic et al. 2008; van Oorschot et al. 2016; Fasshauer et al. 2017; Lassmann et al. 2010; Wang et al. 2016).

Currently, in the context of radiology, irradiation-induced DSBs after computed tomography examinations are analyzed in peripheral blood lymphocytes nuclei using the γ-H2AX immunofluorescence method to visualize the onset of DNA DSB-induced DNA repair (Kuefner et al. 2010b, 2009; Piechowiak et al. 2015; Geisel et al. 2008; Pathe et al. 2011; Deinzer et al. 2014; Reddig et al. 2017). A disadvantage of the method is the fact that the 3D nature of the nucleus is rarely taken into account (Tao et al. 2018; Kuefner et al. 2010a; Piechowiak et al. 2015; Wang et al. 2017). Using epifluorescence microscopy, the entirety of fluorescence signals is visualized as integral without clear delineation of single foci. Therefore, the aim of this study was to use confocal microscopy and 3D reconstructed images to enable improved documentation and analysis of γ-H2AX fluorescence signals in the context of clinical radiology.

Materials and methods

Cell culture and irradiation

MRC-5 cells, primary human fibroblasts, from the lung were purchased from American Type Culture Collection (ATCC, Manassas, VA, USA) and grown, on coverslips, in DMEM/Ham's F-12 (1/1), complemented with 10% fetal bovine serum.

Confluent, non-dividing MRC-5 cells were exposed to the following radiation doses: 0, 200, 300, 400, 500, and 1000 mGy using a Gammacell 40 Exactor with a central dose rate of 1000 mGy/minute at room temperature (Nordion International, Ottawa, Canada). Sham-irradiation was performed as described for the test samples but without irradiation. Exposed samples were kept for 10 min in a humidified incubator (37 °C, 5% CO_2 in air) before fixation with acetone–methanol [1/1 (vol/vol)] for 5 min at − 20 °C.

Blood collection and irradiation

All studies have been done in accordance with the Code of Ethics of the World Medical Association (Declaration of Helsinki) for experiments involving humans. Peripheral venous blood samples of healthy staff volunteers were collected in heparinized tubes (Sarstedt, Nümbrecht, Germany).

Whole blood was exposed in vitro to the following radiation doses of 0, 200, 400, 800, and 1600 mGy by a Gammacell 40 Exactor at room temperature. For control, cells were sham-irradiated in all experiments.

To isolate WBCs, 200 μL blood of each sample after 10 min incubation at 37 °C was mixed with 1 mL eBioscience™ 1-Step Fix/Lyse solution (Thermo Scientific, Weltham, MA, USA Jersey, USA) and incubated for 10 min at RT. WBCs were sedimented in a bench-top centrifuge for 2 min at 480×*g* and washed once with phosphate-buffered saline pH 7.4 (PBS). The WBCs were resuspended in 20 μL PBS, transferred onto a glass cover and were fixed with acetone–methanol [1/1 (vol/vol)] for 5 min at − 20 °C.

Immunofluorescence

Fixed specimens were incubated with monoclonal anti-γ-H2AX Ab (1:500 dilution, Merck Millipore, Billerica, MA, USA) for 1 h at room temperature, washed, and stained using Alexa™ 488-conjugated goat anti-mouse secondary antibody (1:500 dilution, Molecular Probes, Eugene, OR, USA) for 1 h at room temperature in the dark. Cells were washed and incubated with DAPI for 1 min and mounted with Dako fluorescent mounting medium (Dako, Carpinteria, CA, USA).

Microscopy

The 3D distribution of γ-H2AX foci was visualized using confocal laser scanning microscopy with a 63x magnification objective (Zeiss LSM 880 confocal microscope with Airyscan). The nucleus was visualized by DAPI. An Argon 488 nm laser and a 405 nm diode laser were used to acquire images. DAPI was imaged by detection between 410 and 495 nm, and Alexa™ 488 labelled anti-γ-H2AX Ab was detected between 499 and 552 nm. To determine the real number, size, and spatial arrangement of DSBs existing inside it, optical slices with 600 nm intervals were performed (scaling per pixel: 0.290 μm × 0.290 μm × 0.608 μm). For each field of view about 25–35 optical slices were usually obtained and used for either maximal intensity projections or 3D reconstructions. Maximum intensity projection was performed of Z-stacks by Zeiss Zen software (Carl Zeiss AG, Oberkochen, Germany). In addition, γ-H2AX foci were visualized by epifluorescence microscopy (Zeiss Axiovert microscope).

3D reconstruction

Acquired confocal Z-stacks comprising up to 35 images were reconstructed into 3D using Imaris image analysis

software (Bitplane AG, Zurich, Switzerland). The volumes of the nuclei (DAPI) and of the γ-H2AX (Alexa™ 488) foci were segmented using the absolute intensity threshold whose identification is of crucial importance. Nuclear and γ-H2AX volumes were obtained separately. Touching objects were split by the calculated seed points inside each area.

Quantification of γ-H2AX foci

For quantification of γ-H2AX foci by confocal microscopy plus 3D reconstruction, a field of ≥ 20 nuclei stained by DAPI only was selected to exclude bias. Parameters used for DNA DSB-counts and of the number of nuclei as well (seed points, intensity, and number of voxels) were kept constant, within one series of experiments, for all radiation doses. Touching objects were separated with a guide size of 0.5 μm; however, filter-type quality varied, and were adjusted for optimal signal/noise ratios. Further, foci were counted of a maximum projection image by eye.

In parallel, γ-H2AX foci were counted visually by epifluorescence microscopy through the ocular. A field of about 20 nuclei was selected by DAPI staining as above. Four people blinded for the experimental design counted the γ-H2AX foci visually.

Results

Microscopy

DNA DSBs (green signal) were examined by confocal microscopy and by epifluorescence microscopy after an irradiation dose of 1000 mGy. Using confocal microscopy, all induced DSBs identifiable in the nucleus (blue signal) were displayed. They resided on different Z-planes. In contrast, by epifluorescence microscopy the entirety of fluorescence signals was visualized as integral without clear demarcation of single foci (Fig. 1).

We investigated the induction of DSBs in confluent cultures of primary MRC-5 fibroblasts exposed to increasing radiation doses. As shown in Fig. 2, the visible increase in γ-H2AX foci initially correlates with the applied radiation dose.

3D reconstruction

The Z-stacks obtained by confocal microscopy were used for the reconstruction and segmentation of cell nuclei and γ-H2AX foci volumes shown in Fig. 3. Seed points (white spheres) were calculated within each surface to split objects and were used for 3D counting analysis. The visible seed points in Fig. 3c, represent γ-H2AX foci and were used for DSB quantification.

Quantification of γ-H2AX

To test DSB quantification using confocal microscopy, γ-H2AX foci were counted with the Imaris software after 3D reconstruction as described. In parallel, images were counted visually of the same irradiated samples using an epifluorescence microscope. Dose–response curves for γ-H2AX foci in irradiated MRC-5 cells up to 1000 mGy was obtained by confocal microscopy plus 3D reconstruction, by maximum intensity projection images of the optical slices or by an epifluorescence microscope analysis (Fig. 4). Comparison shows that the mean number of DSBs per nucleus counted by Imaris software after 3D reconstruction yields higher DSBs/nucleus than determined visually (Table 1; Fig. 4.). The average number determined by epifluorescence microscope for 200 mGy, was 2.4 ± 0.8 DSBs per cell nucleus. At 500 mGy and 1000 mGy exposure, 6.7 ± 2.0 and 11.1 ± 2.1 DSBs were counted per cell nucleus, respectively. In contrast, in two independent experiments the 3D distribution of γ-H2AX foci counted by Imaris software yielded an average number of 13.8 ± 1.6 DSBs per cell nucleus for 200 mGy. An average of 23 ± 4.2 DSBs were counted by 500 mGy and 36.1 ± 3.5 DSBs per

Fig. 1 Irradiated MRC-5 fibroblasts were fixed and DSBs were detected by anti- γ-H2AX indirectly. Nuclei were visualized by DAPI. **a** Optical slices with 600 nm intervals of a single nucleus were performed by confocal microscopy to visualize the whole nuclei. **b** Epifluorescence microscopy visualized the fluorescence signals in their entirety as integral without correct demarcation of single foci
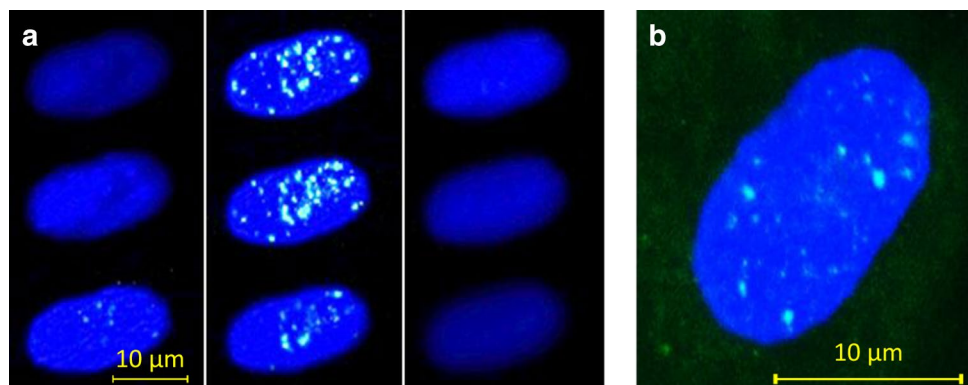
Fig. 2 Growth-arrested MRC-5 fibroblasts cultures were exposed to incremental radiation doses. The specimens show a dose-dependent increase in the density of γ-H2AX foci
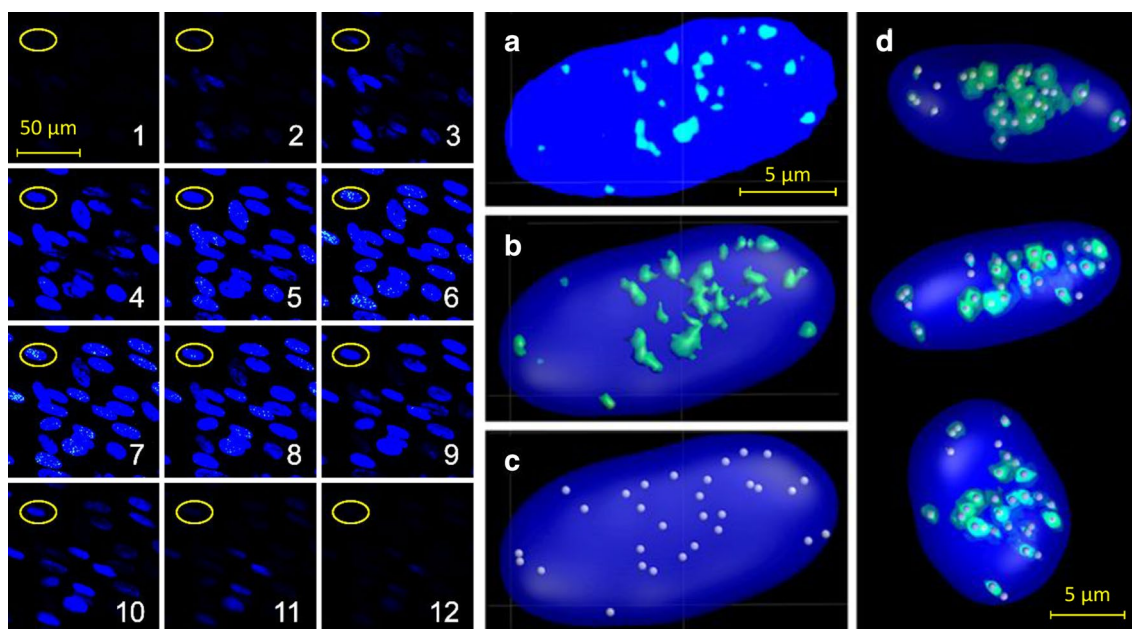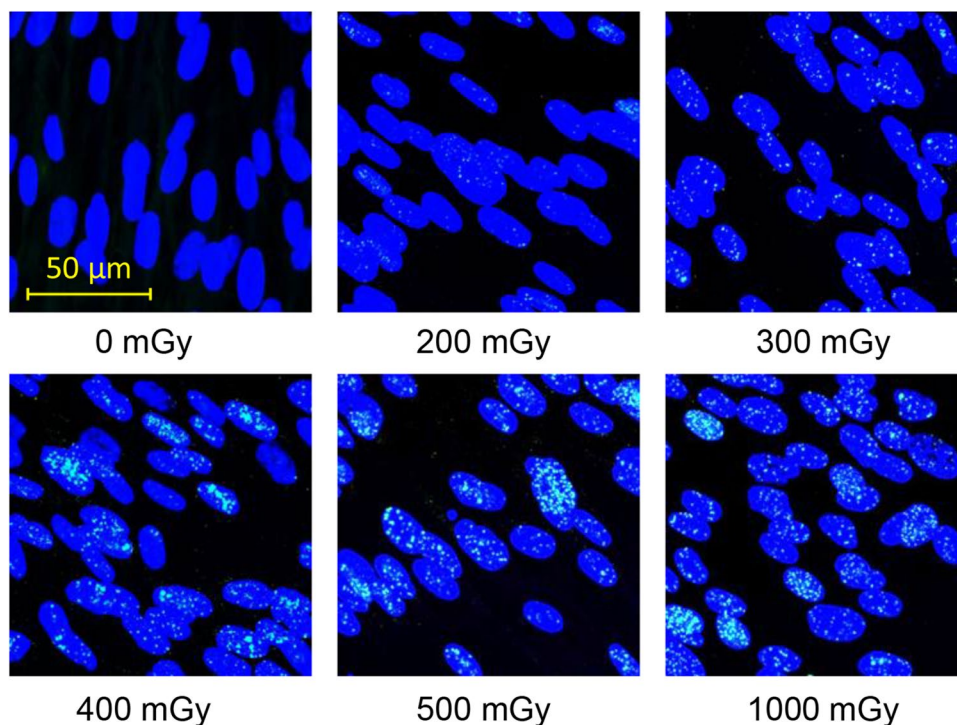

Fig. 3 Representative Z-stack images captured by confocal microscopy (1–12) were reconstructed to a 3D image using the Imaris software. The yellow circled nucleus shown in the Z-stacks is magnified as an example for the 3D reconstruction. The nucleus is depicted in blue. In green are shown the γ-H2AX foci or groups thereof. The white spheres represent the seed points of anti-γ-H2AX fluorescence. **a** Top view of the nucleus, **b, c** 3D views of the foci and seed points within the nucleus, respectively. Exemplary representations of the same nucleus as used in **a–c** as seen from various angles are depicted in (**d**)

cell nucleus by 1000 mGy. When the number of γ-H2AX foci was analyzed by maximum intensity projection images, an average number of 4.4 ± 1.9 DSBs per cell nucleus was counted for 200 mGy. An average of 12.4 ± 4.1 DSBs were counted by 500 mGy and 17.4 ± 3.0 DSBs per cell nucleus by 1000 mGy.
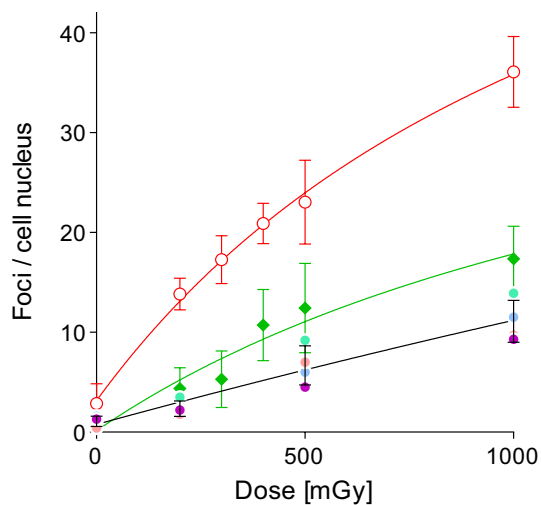
Fig. 4 MRC-5 cells were irradiated with 0, 200, 300, 400, 500 or 1000 mGy, incubated (37 °C) for 10 min, and fixed with acetone/methanol. Immunofluorescence staining was performed as described. By confocal microscopy fields of approx. 20 nuclei were selected based on DAPI staining only to exclude bias. 3D reconstruction and counting of foci (red circles) were performed as described. Further, foci were counted from maximum intensity projection images by eye (green diamonds) In addition, imaging with a epifluorescence microscope was performed, and the images were given to four persons blinded for the enumeration of foci (colored dots/lines green circles, blue circles, pink circles, purple circles individual results, black: mean value). All curves were obtained by non-linear, sigmoid curve fitting (dose–response curve)

In addition, the ratio between confocal microscopy and 3D reconstruction and epifluorescence microscope was calculated. The ratio for 200 mGy was 5.8 ± 2.0. A 3.4 ± 1.2 fold higher number of DSBs compared to epifluorescence microscopy was calculated for 500 mGy. At 1000 mGy exposure the calculated ratio was 3.3 ± 0.7.

Comparison of the values obtained by 3D reconstructed images with foci counted on major intensity projection images or the numbers resulting from epifluorescence microscopy by statistical means clearly showed that except for the non-irradiated samples the numbers were significantly different. Statistical analysis was carried out using

a multiple unpaired t test on the two curves and statistical significance was determined using the Holm–Sidak method, with alpha $= 0.05$ (Holm 1979). The p values obtained were > 0.3 for the non-irradiated cells and < 0.001 for the irradiated cells, respectively (Table 1).

Moreover, the quantification of DNA DSB foci by confocal microscopy followed by 3D reconstruction may be used as biologic dosimeter for radiation exposure. To this end, blood samples were irradiated in the dose range from 0.2 to 1.6 Gy and stained for γ-H2AX. Acquired image stacks were 3D reconstructed, and γ-H2AX foci were counted using Imaris software (Fig. 5a). An average of 1.1 ± 0.8 DSBs were counted by 200 mGy, 3.3 ± 1.7 DSBs per cell nucleus by 400 mGy, 8.9 ± 3.1 DSBs per cell nucleus by 800 mGy and 18.4 ± 0.8 DSBs per cell nucleus by 1600 mGy. In parallel, γ-H2AX foci were counted visually by epifluorescence microscopy. An average number of 1.2 ± 0.3 DSBs per cell nucleus was counted for 200 mGy, 1.7 ± 0.4 DSBs were counted by 400 mGy, 3.17 ± 0.6 DSBs were counted by 800 mGy and 5.6 ± 1.9 DSBs per cell nuclei by 1600 mGy. Dose–response curves for γ-H2AX foci in irradiated WBCs obtained by confocal microscopy plus 3D reconstruction or by an epifluorescence microscope are shown in Fig. 5b.

Discussion

Genotoxicity is a wide field ranging from desired DNA DSB in malignant cells to kill them to unwanted effects of chemical compounds including drugs and physical influences such as irradiation and heat for example. To objectively estimate the genotoxicity of different origin, its extent can be quantified by counting the number of visible γ-H2AX foci. In a medical context (e.g., computer tomography), DNA DSBs may produce genetic instability and represent the most significant lesions after exposure to ionizing radiation.

However, previous approaches to study radiation-induced DSBs after diagnostic examinations neglected the 3D nature of the nucleus. In epifluorescence microscopy the entire

Table 1 γ-H2AX foci analysis on different doses of radiation in MRC-5 cells

| Dose (mGy) | Foci/cell nucleus (mean ± SD) | | | Difference | | | |
| | Confocal microscopy & | | | 3DR / CFM | | MIP / 3DR | |
	Conventional fluorescence microscopy (CMF)	3D reconstruction (3DR)	Maximum intensity projection (MIP)	Significant*	p	Significant*	p
0	1.1 ± 0.5	2.9 ± 2.0	0.8 ± 0.5	No	0.309	No	0.328
200	2.4 ± 0.8	13.8 ± 1.6	4.4 ± 1.9	Yes	< 0.001	Yes	< 0.001
500	6.7 ± 2.0	23 ± 4.2	12.4 ± 4.1	Yes	< 0.001	Yes	< 0.001
1000	11.1 ± 2.1	36.1 ± 3.5	17.4 ± 3.0	Yes	< 0.001	Yes	< 0.001

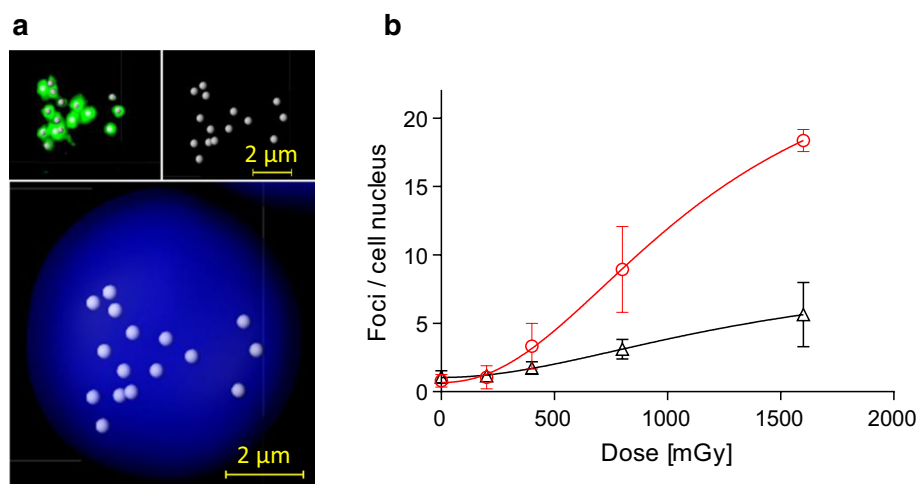*Statistical significance was determined using the Holm-Sidak method, with $\alpha = 0.05$

Fig. 5 Whole blood was irradiated with 0, 200, 400, 800 or 1600 mGy, and incubated (37 °C) for 10 min. WBCs were isolated and the γ-H2AX analysis was performed by confocal microscopy and by epifluorescence microscope. **a** Fields of approx. 20 nuclei were selected based on DAPI staining only to exclude bias. 3D reconstruction and counting of Foci were done as described. **b** Shows dose response curves of WBCs analyzed by confocal microscopy plus 3D reconstruction red circles and by epifluorescence microscope triangle. Curves were obtained by non-linear, sigmoid curve fitting (dose response curve)

field of the nucleus is simultaneously illuminated by light and visualized. The illumination of other parts of the specimen results in background noise, which affects the quality of the image (Nwaneshiudu et al. 2012). As a consequence γ-H2AX foci outside the focal point of the objective lens of the microscope are not taken into account.

In contrast, confocal microscopy plus 3D imaging enable a more realistic determination of number, size, and spatial arrangement of the γ-H2AX foci present. The significant difference in DSB counts per cell nucleus after irradiation between these two methods was shown in Fig. 4. Furthermore, the counting of DSBs/cell nucleus is independent of the person evaluating.

In the present study, we show the improved γ-H2AX assay on the basis of confocal microscopy and 3D image reconstructions. This improved assay does not simply identify foci in each Z-plane and count them on maximum intensity projection images as described elsewhere (Markova et al. 2007; Borras et al. 2015; Vasireddy et al. 2010). Projecting an object from a 3D volume to a 2D plane always results in information loss (Shihavuddin et al. 2017). Comparison of the values obtained by 3D reconstructed images with the numbers resulting from maximum intensity projection images showed that except for the non-irradiated samples the numbers were significantly higher (Fig. 3). Foci analysis by Rothkamm et al. of irradiated MRC-5 cells with 200 mGy after 15 min incubation time from maximum intensity projection images resulted in about 5 foci per cell nuclei (Rothkamm and Lobrich 2003). The value in the present study with 4.4 ± 1.9 foci per nuclei (Table 1), fully matches this result. The value at 200 mGy obtained by 3D

reconstructed images was higher with 13.8 ± 1.6 foci per cell nuclei.

A further method of analysis, a so called pseudo 3D counting was described by Ivashkevich and collaborators (Ivashkevich et al. 2011). They showed that this method based on confocal microscopy and subsequent application of a mathematic algorithm (pseudo 3D counting) resulted in approximately the double number of DSBs compared with the conventional method. The method described in the current study, however, results in a 3.3–5.8 fold higher number of DSBs compared to epifluorescence microscopy and doesn't require an algorithm to analyse overlapping objects in adjacent Z-planes.

The calculated ratio between confocal microscopy plus 3D reconstruction and epifluorescence microscopy revealed that the ratio is not uniform with increasing irradiation doses. Therefore, counted γ-H2AX foci by epifluorescence microscopy cannot be simply adjusted by multiplying the determined DSBs by a uniform factor. It displays all existing γ-H2AX foci and excludes overlapping by 3D reconstructed images.

In biological dosimetry, exact analysis of induced γ-H2AX foci is relevant. A discrepancy was observed in foci numbers in MRC-5 fibroblasts between counts made on maximum intensity projection images and those generated with Imaris/3D reconstruction. Foci analysis in WBC's by the described method enables an improved study of the effects of ionizing radiation, with 2 to threefold higher number of DSBs compared to epifluorescence microscopy. Quantitatively similar results has been published for z-stack maximum projections of confocal sections (Ivashkevich

et al. 2011). However, in contrast to the results presented herein the study of Ivashkevich et al. analyzed DSBs only in enriched lymphocytes obtained from whole blood. γ-H2AX signal is present in all nucleated white blood cells, however, the distribution of γ-H2AX signal may vary between nucleated blood cell types. The study of Ismail et al. showed 3 times higher level of γ-H2AX signal in B-lymphocytes than in unsorted WBC (Ismail et al. 2007). Hence, we would expect an increase in the number of DSB foci if only lymphocytes were analyzed with Imaris/3D reconstruction. Our method may increase the accuracy and sensitivity of identifying radiation mediated DNA damage after diagnostic examinations such as computed tomography. Our study shows a sigmoid dose–response curves in MRC-5 fibroblasts and in WBC's as observed elsewhere [(Wojewodzka et al. 2015), unfitted data from Fig. 3b].

Taken together, these findings enable improved documentation and analysis of genotoxic radiation effects. Thus representing a new, sensitive and reliable research tool, which may increase the accuracy and sensitivity of identifying radiation mediated DNA damage in future patient care.

References

Berrington de Gonzalez A, Darby S (2004) Risk of cancer from diagnostic X-rays: estimates for the UK and 14 other countries. Lancet 363(9406):345–351. https://doi.org/10.1016/S0140-6736(04)15433-0

Borras M, Armengol G, De Cabo M, Barquinero JF, Barrios L (2015) Comparison of methods to quantify histone H2AX phosphorylation and its usefulness for prediction of radiosensitivity. Int J Radiat Biol 91(12):915–924. https://doi.org/10.3109/09553002.2015.1101501

Burma S, Chen BP, Murphy M, Kurimasa A, Chen DJ (2001) ATM phosphorylates histone H2AX in response to DNA double-strand breaks. J Biol Chem 276(45):42462–42467. https://doi.org/10.1074/jbc.C100466200

Chen HT, Bhandoola A, Difilippantonio MJ, Zhu J, Brown MJ, Tai X, Rogakou EP, Brotz TM, Bonner WM, Ried T, Nussenzweig A (2000) Response to RAG-mediated VDJ cleavage by NBS1 and gamma-H2AX. Science 290(5498):1962–1965

Deinzer CK, Danova D, Kleb B, Klose KJ, Heverhagen JT (2014) Influence of different iodinated contrast media on the induction of DNA double-strand breaks after in vitro X-ray irradiation. Contrast

Media Mol Imaging 9(4):259–267. https://doi.org/10.1002/cmmi.1567

Fasshauer M, Kruwel T, Zapf A, Stahnke VC, Rave-Frank M, Staab W, Sohns JM, Steinmetz M, Unterberg-Buchwald C, Schuster A, Ritter C, Lotz J (2017) Absence of DNA double-strand breaks in human peripheral blood mononuclear cells after 3 T magnetic resonance imaging assessed by gammaH2AX flow cytometry. Eur Radiol. https://doi.org/10.1007/s00330-017-5056-9

Geisel D, Heverhagen JT, Kalinowski M, Wagner HJ (2008) DNA double-strand breaks after percutaneous transluminal angioplasty. Radiology 248(3):852–859. https://doi.org/10.1148/radiol.2483071686

Holm S (1979) A Simple Sequentially Rejective Multiple Test Procedure Scandinavian. Journal of Statistics 6(2):65–70

Ismail IH, Wadhra TI, Hammarsten O (2007) An optimized method for detecting gamma-H2AX in blood cells reveals a significant interindividual variation in the gamma-H2AX response among humans. Nucleic Acids Res 35(5):e36. https://doi.org/10.1093/nar/gkl1169

Ivashkevich AN, Martin OA, Smith AJ, Redon CE, Bonner WM, Martin RF, Lobachevsky PN (2011) gammaH2AX foci as a measure of DNA damage: a computational approach to automatic analysis. Mutat Res 711(1–2):49–60. https://doi.org/10.1016/j.mrfmmm.2010.12.015

Kuefner MA, Grudzenski S, Schwab SA, Wiederseiner M, Heckmann M, Bautz W, Lobrich M, Uder M (2009) DNA double-strand breaks and their repair in blood lymphocytes of patients undergoing angiographic procedures. Investig Radiol 44(8):440–446. https://doi.org/10.1097/RLI.0b013e3181a654a5

Kuefner MA, Grudzenski S, Hamann J, Achenbach S, Lell M, Anders K, Schwab SA, Haberle L, Lobrich M, Uder M (2010a) Effect of CT scan protocols on X-ray-induced DNA double-strand breaks in blood lymphocytes of patients undergoing coronary CT angiography. Eur Radiol 20(12):2917–2924. https://doi.org/10.1007/s00330-010-1873-9

Kuefner MA, Hinkmann FM, Alibek S, Azoulay S, Anders K, Kalender WA, Achenbach S, Grudzenski S, Lobrich M, Uder M (2010b) Reduction of X-ray induced DNA double-strand breaks in blood lymphocytes during coronary CT angiography using high-pitch spiral data acquisition with prospective ECG-triggering. Investig Radiol 45(4):182–187. https://doi.org/10.1097/RLI.0b013e3181d3eddf

Lassmann M, Hanscheid H, Gassen D, Biko J, Meineke V, Reiners C, Scherthan H (2010) In vivo formation of gamma-H2AX and 53BP1 DNA repair foci in blood cells after radioiodine therapy of differentiated thyroid cancer. J Nucl Med 51(8):1318–1325. https://doi.org/10.2967/jnumed.109.071357

Lobrich M, Jeggo PA (2007) The impact of a negligent G2/M checkpoint on genomic instability and cancer induction. Nat Revi Cancer 7(11):861–869. https://doi.org/10.1038/nrc2248

Markova E, Schultz N, Belyaev IY (2007) Kinetics and dose-response of residual 53BP1/gamma-H2AX foci: co-localization, relationship with DSB repair and clonogenic survival. Int J Radiat Biol 83(5):319–329. https://doi.org/10.1080/09553000601170469

Muslimovic A, Ismail IH, Gao Y, Hammarsten O (2008) An optimized method for measurement of gamma-H2AX in blood mononuclear and cultured cells. Nat Protoc 3(7):1187–1193. https://doi.org/10.1038/nprot.2008.93

Nwaneshiudu A, Kuschal C, Sakamoto FH, Anderson RR, Schwarzenberger K, Young RC (2012) Introduction to confocal microscopy. J Investig Dermatol 132(12):e3. https://doi.org/10.1038/jid.2012.429

Pathe C, Eble K, Schmitz-Beuting D, Keil B, Kaestner B, Voelker M, Kleb B, Klose KJ, Heverhagen JT (2011) The presence of iodinated contrast agents amplifies DNA radiation damage in

computed tomography. Contrast Media Mol Imaging 6(6):507–513. https://doi.org/10.1002/cmmi.453

Piechowiak EI, Peter JF, Kleb B, Klose KJ, Heverhagen JT (2015) Intravenous iodinated contrast agents amplify DNA radiation damage at CT. Radiology 275(3):692–697. https://doi.org/10.1148/radiol.14132478

Pilch DR, Sedelnikova OA, Redon C, Celeste A, Nussenzweig A, Bonner WM (2003) Characteristics of gamma-H2AX foci at DNA double-strand breaks sites. Biochem Cell Biol Biochimie et biologie cellulaire 81 (3):123–129. https://doi.org/10.1139/o03-042

Reddig A, Fatahi M, Roggenbuck D, Ricke J, Reinhold D, Speck O, Friebe B (2017) Impact of in vivo high-field-strength and ultra-high-field-strength MR imaging on DNA double-strand-break formation in human lymphocytes. Radiology 282(3):782–789. https://doi.org/10.1148/radiol.2016160794

Rogakou EP, Pilch DR, Orr AH, Ivanova VS, Bonner WM (1998) DNA double-stranded breaks induce histone H2AX phosphorylation on serine 139. J Biol Chem 273(10):5858–5868

Rothkamm K, Lobrich M (2003) Evidence for a lack of DNA double-strand break repair in human cells exposed to very low X-ray doses. Proc Natl Acad Sci USA 100(9):5057–5062. https://doi.org/10.1073/pnas.0830918100

Sedelnikova OA, Rogakou EP, Panyutin IG, Bonner WM (2002) Quantitative detection of (125)IdU-induced DNA double-strand breaks with gamma-H2AX antibody. Radiat Res 158(4):486–492

Shihavuddin A, Basu S, Rexhepaj E, Delestro F, Menezes N, Sigoillot SM, Del Nery E, Selimi F, Spassky N, Genovesio A (2017) Smooth 2D manifold extraction from 3D image stack. Nat Commun 8:15554. https://doi.org/10.1038/ncomms15554

Stiff T, O'Driscoll M, Rief N, Iwabuchi K, Lobrich M, Jeggo PA (2004) ATM and DNA-PK function redundantly to phosphorylate H2AX after exposure to ionizing radiation. Cancer Res 64(7):2390–2396

Symington LS, Gautier J (2011) Double-strand break end resection and repair pathway choice. Annu Re Genet 45:247–271. https://doi.org/10.1146/annurev-genet-110410-132435

Tao SM, Li X, Schoepf UJ, Nance JW Jr, Jacobs BE, Zhou CS, Gu HF, Lu MJ, Lu GM, Zhang LJ (2018) Comparison of the effect of radiation exposure from dual-energy CT versus single-energy CT on double-strand breaks at CT pulmonary angiography. Eur J Radiol 101:92–96. https://doi.org/10.1016/j.ejrad.2018.02.002

Tounekti O, Kenani A, Foray N, Orlowski S, Mir LM (2001) The ratio of single- to double-strand DNA breaks and their absolute values determine cell death pathway. Br J Cancer 84(9):1272–1279. https://doi.org/10.1054/bjoc.2001.1786

van Oorschot B, Hovingh S, Dekker A, Stalpers LJ, Franken NA (2016) Predicting radiosensitivity with gamma-H2AX foci assay after single high-dose-rate and pulsed dose-rate ionizing irradiation. Radiat Res 185(2):190–198. https://doi.org/10.1667/RR14098.1

Vasireddy RS, Tang MM, Mah LJ, Georgiadis GT, El-Osta A, Karagiannis TC (2010) Evaluation of the spatial distribution of gammaH2AX following ionizing radiation. J Vis Exp JoVE. https://doi.org/10.3791/2203

Wang H, Wang M, Bocker W, Iliakis G (2005) Complex H2AX phosphorylation patterns by multiple kinases including ATM and DNA-PK in human cells exposed to ionizing radiation and treated with kinase inhibitors. J Cell Physiol 202(2):492–502. https://doi.org/10.1002/jcp.20141

Wang J, Yin L, Zhang J, Zhang Y, Zhang X, Ding D, Gao Y, Li Q, Chen H (2016) The profiles of gamma-H2AX along with ATM/DNA-PKcs activation in the lymphocytes and granulocytes of rat and human blood exposed to gamma rays. Radiat Environ Biophys 55(3):359–370. https://doi.org/10.1007/s00411-016-0653-6

Wang L, Li Q, Wang XM, Hao GY, Jie B, Hu S, Hu CH (2017) Enhanced radiation damage caused by iodinated contrast agents during CT examination. Eur J Radiol 92:72–77. https://doi.org/10.1016/j.ejrad.2017.04.005

Ward IM, Chen J (2001) Histone H2AX is phosphorylated in an ATR-dependent manner in response to replicational stress. J Biol Chem 276(51):47759–47762. https://doi.org/10.1074/jbc.C100569200

Wojewodzka M, Sommer S, Kruszewski M, Sikorska K, Lewicki M, Lisowska H, Wegierek-Ciuk A, Kowalska M, Lankoff A (2015) Defining blood processing parameters for optimal detection of gamma-H2AX Foci: a small blood volume method. Radiat Res 184(1):95–104. https://doi.org/10.1667/RR13897.1